Research Article

Deformation and Stability Analysis of a Core Rockfill Dam with Leakage

Yuanzhong Chen,[1] Guobing Lin,[1] and Yangyang Lu [2]

[1]*Shenzhen Gongming Water Supply and Storage Engineering Management, Shenzhen 518107, China*
[2]*Geotechnical Engineering Department, Nanjing Hydraulic Research Institute, Nanjing 210024, China*

Correspondence should be addressed to Yangyang Lu; yylu@nhri.cn

The No. 4 clay core rockfill dam of the Gongming Reservoir experienced leakages when the reservoir water level was low. To analyze the leakage causes, a series of seepage tests were conducted on the dam materials in this paper. And a three-dimensional finite element stress-seepage coupled calculation model of the dam was established to study the deformation and stresses of the dam under the condition of normal storage water level and the sharp drop in the storage level. The test results show that the permeability coefficient of the clay core material is close to that of the dam shell material, resulting in the leakage of the dam under the condition of the low-water level. The simulation results show that the dam deforms a little under the condition of normal storage water level and the sharp drop in the storage level, and the stress distribution under the condition of the sharp drop in the storage level is basically consistent with that under the condition of normal storage water level. The safety factors of the dam under the two conditions meet the requirements of the specification, but the margin of the safety factor is small.

1. Introduction

The Earth rock dam, which has the advantages of good terrain adaptability, usage of local materials, low investment, and simple construction, is one of the main dam types for hydropower development and dam construction in China [1–3]. The seepage stability has always been one of the core issues in the safe construction and operation of Earth rock dams [4–7]. When the reservoir water level rises or falls suddenly, the seepage field in the dam changes greatly in a short time, affecting the stability of the dam, especially for the upstream slope of the dam. For this reason, researchers and technicians have done a lot of work on the aspects of anti-seepage technology, dam safety monitoring methods, and Earth rock dam disease mechanism to solve the problem of dam leakage [8–11]. However, due to the limitation of the technical level during the construction period or the comprehensive impact of the later transportation and maintenance, there are still hidden dangers in the seepage stability of a large number of reservoir dams.

The three-dimensional finite element stress-seepage coupled calculation method is a preferred method to study the dam instability caused by seepage, and the method has been widely used in the analysis of the deformation and stability of Earth rock dams [12–15]. However, only are the Earth rock dams in the design stage or in safe operation mentioned in previous studies, but the Earth rock dam with leakage has not been studied yet. During the routine inspection of Gongming Reservoir in Shenzhen, China, it was found that the No. 4 clay core rockfill dam leakages were experienced even under the low-water level operation (i.e., the water level was lower than the design normal storage water level). To ensure the safe operation of the No. 4 clay core rockfill dam, it is necessary to find out the causes of leakage of the dam and study its deformation and stability under the condition of normal storage water level and the sharp drop in the storage level.

In this paper, a series of seepage tests were first carried out to analyze the causes of dam leakage, then a three-dimensional finite element stress-seepage coupled

calculation model of the dam was established to study the deformation and stresses of the dam under the condition of normal storage water level and the sharp drop in the storage level. On the basis of the finite element calculation results, the stability of the dam is analyzed using Bishop's slice method.

2. Project Overview

Gongming Reservoir is located northwest of Shenzhen, China. The total storage capacity of the storage reservoir is 148 million m³. The design flood level of the reservoir is 60.68 m, the checking flood level of the dam is 60.96 m, the normal water storage level is 59.70 m, and the dead water level is 26.50 m. The main buildings include the reservoir dam, spillway, water discharge tunnel, connecting tunnel, water supply tunnel, etc.

The No. 4 dam of Gongming Reservoir is a clay core rockfill dam (as shown in Figure 1), with a crest length of 1121.1 m, a crest elevation of 63.50 m, and a maximum dam height of 50.70 m. A 2 m wide berm is set downstream. The dam slope above the berm is 1 : 2.5, and the dam slope below the berm is 1 : 2.75. A rockfill drainage prism is set at the dam toe, and the top elevation of the rockfill prism is 25 m. Downstream of the prism, a drainage ditch and a measuring weir are laid. The top width of the clay anti-seepage core wall in the dam is 6.0 m, and the ratio of upstream and downstream slopes is 1 : 0.5. A sand filter layer with a thickness of 2 m is set between the clay core wall and the downstream dam shell. A sand filter layer with a thickness of 1 m is set between the clay core wall and upstream shell. The anti-seepage wall and curtain grouting are set in the dam for blocking seepage. The thickness of the concrete anti-seepage wall is 600 mm, and the lower end of the wall is embedded with 0.5 m of strongly weathered rock. According to the Chinese classification and flood standard for water resources and hydropower projects, the No. 4 dam project is classified as class II.

In February 2018, it was found that the No. 4 dam leakages were experienced in many sections when the reservoir water level was 40.25 m, which was less than the normal water level of 59.70 m, as shown in Figure 2. It can be seen that fine sands flow out of individual leakage points, and the seepage drainage volume increased significantly, which may not be conducive to the safety of the dam. Piezometers and inclinometer pipes were also installed in the dam. The piezometer is mainly arranged at the dam upstream of the core wall (P-1), the centerline of the core wall (P-2), the downstream edge of the core wall (P-3), and the dam under the downstream berm of each section (P-4). The inclinometer pipe is arranged at the dam toe (IP-0), as shown in Figure 1. Figure 3 shows the measured saturation line in the dam when the upstream water level is 45.0 m. The saturation line gradually decreases from upstream to downstream, which is in line with the general law of seepage of the Earth rock dam. However, the measured value of P-4 located in the downstream dam is 27.94 m, which is higher than the top of the downstream drainage prism of the dam

(25.00 m), which indicated that the saturation line in the dam is high.

3. Seepage Tests and Test Results

To find out the causes of the dam leakages, a series of laboratory seepage tests on the materials in each area of the dam were conducted to obtain their permeability coefficients. The sampling work is shown in Figure 4. A variable head device was used to obtain the permeability coefficients of the samples. Table 1 gives the permeability coefficients of the materials in each area of the dam. It can be seen that the permeability coefficient of the core material is close to that of dam shell material, indicating that the No. 4 core rockfill dam is close to that of a homogeneous dam. According to the Chinese standard (SL 274-2020), homogeneous dams are mostly used for low dams (dam height is less than 30 m), while the No. 4 dam in Gongming Reservoir has a maximum height of 50.7 m, which is already a medium dam. In addition, the prism drainage arranged downstream of the dam has been submerged by the downstream water level of the dam. Therefore, even if the reservoir water level is low, the saturation surface of the dam is still high, resulting in leakage at multiple sections of the dam.

4. Stress-Seepage Coupled Model

In this section, the stress-seepage coupled model to analyze the deformation and stresses of the No. 4 dam is established based on the Biot consolidation theory [16]. Its equation is derived from the equilibrium differential equation of forces, effective stress principle, constitutive equation, geometric equation, and continuity equation.

4.1. Equilibrium Differential Equation of Forces. Take a soil element in the dam, and the equilibrium differential equation of its force is

$$\frac{\partial \sigma_x}{\partial x} + \frac{\partial \tau_{xy}}{\partial y} + \frac{\partial \tau_{xz}}{\partial z} = f_x,$$

$$\frac{\partial \tau_{xy}}{\partial x} + \frac{\partial \sigma_y}{\partial y} + \frac{\partial \tau_{yz}}{\partial z} = f_y, \quad (1)$$

$$\frac{\partial \tau_{xz}}{\partial x} + \frac{\partial \tau_{yz}}{\partial y} + \frac{\partial \sigma_z}{\partial z} = f_z,$$

where σ_x, σ_y, σ_z, τ_{xy}, τ_{xz}, and τ_{xz} are the stress components acting on the element, f_x, f_y, and f_z are the components of volume stress in x, y, and z directions, respectively.

4.2. Principle of Effective Stress. According to the principle of effective stress, the total stress on the soil element is the sum of effective stress and pore water pressure, and the pore
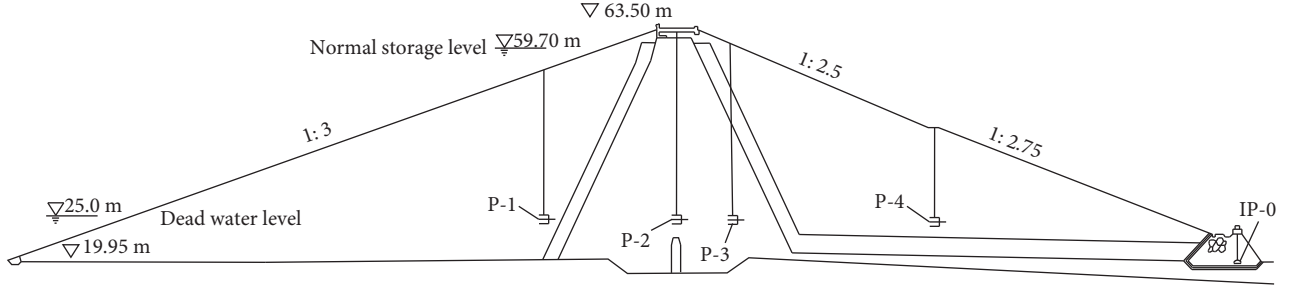
FIGURE 1: Dam section and layout of piezometers and inclinometer pipes.

FIGURE 2: Photos of the dam leakage.

water pressure does not bear shear stress. Its equilibrium equation is expressed as

$$\frac{\partial \sigma'_x}{\partial x} + \frac{\partial \tau_{xy}}{\partial y} + \frac{\partial \tau_{xz}}{\partial z} + \frac{\partial u}{\partial x} = f_x,$$

$$\frac{\partial \tau_{xy}}{\partial x} + \frac{\partial \sigma'_y}{\partial y} + \frac{\partial \tau_{yz}}{\partial z} + \frac{\partial u}{\partial y} = f_y, \tag{2}$$

$$\frac{\partial \tau_{xz}}{\partial x} + \frac{\partial \tau_{yz}}{\partial y} + \frac{\partial \sigma'_z}{\partial z} + \frac{\partial u}{\partial z} = f_z,$$

where μ is the pore pressure component acting on the element, $\sigma'x$, $\sigma'y$, and $\sigma'z$ are the components of effective stress in x, y, and z directions, respectively.

4.3. Constitutive Equation. The constitutive equation is used to describe the relationship of the effective stress $[\sigma']$ and the soil skeleton strain $[\varepsilon]$. Its equilibrium equation is expressed as

$$[\sigma'] = [D][\varepsilon], \tag{3}$$

where $[D]$ is the stiffness tensor of the stress-strain relationship. Here, the constitutive models used are the elastoplastic model developed by Duncan-Chang and the linear elastic model.

4.4. Geometric Equation. Under the assumption of small deformation, the geometric equation is expressed as

$$\varepsilon_x = \frac{\partial w_x}{\partial x}\varepsilon_{yz}$$

$$= \frac{\partial w_y}{\partial z} + \frac{\partial w_z}{\partial y},$$

$$\varepsilon_y = \frac{\partial w_y}{\partial y}\varepsilon_{xz}$$

$$= \frac{\partial w_x}{\partial z} + \frac{\partial w_z}{\partial x}, \tag{4}$$

$$\varepsilon_z = \frac{\partial w_z}{\partial z}\varepsilon_{xy}$$

$$= \frac{\partial w_x}{\partial y} + \frac{\partial w_y}{\partial x},$$

where w_x, w_y, and w_z are the components of the displacement w of the element in x, y, and z directions, respectively.

4.5. Continuity Equation. Under the assumption of small deformation, the geometric equation is expressed as

$$\frac{\partial}{\partial t}\left(\frac{\partial w_x}{\partial x} + \frac{\partial w_y}{\partial y} + \frac{\partial w_z}{\partial z}\right) = -\frac{K}{\gamma_w}\left(\frac{\partial^2 u}{\partial x^2} + \frac{\partial^2 u}{\partial y^2} + \frac{\partial^2 u}{\partial z^2}\right), \tag{5}$$

where K is the permeability coefficient and γ_w is the density of the element.

Solving simultaneous equations (1)–(5), the differential equations for displacement (w_x, w_y, and w_z) and pore water pressure μ can be obtained:

$$\tag{6}$$

5. FEM Simulation and Result Analysis

5.1. Realization of Stress-Seepage Coupled in FEM. The basic idea of the finite element method (FEM) to solve the stress-seepage coupled equation is as follows: (i) discretize the calculation area into a combination of several finite elements; (ii) take an appropriate weight function to characterize the distribution law of pore pressure and displacement inside the unit; (iii) based on the basic differential equations and definite solution conditions,
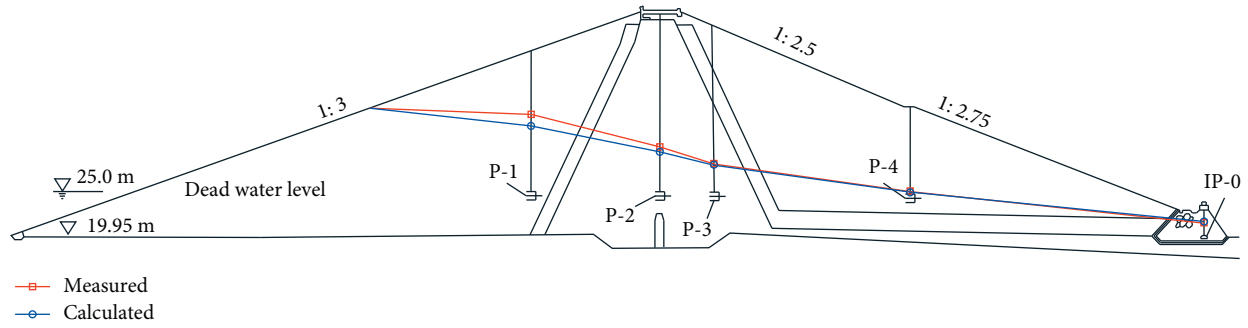
FIGURE 3: Measured and calculated phreatic line of the dam.
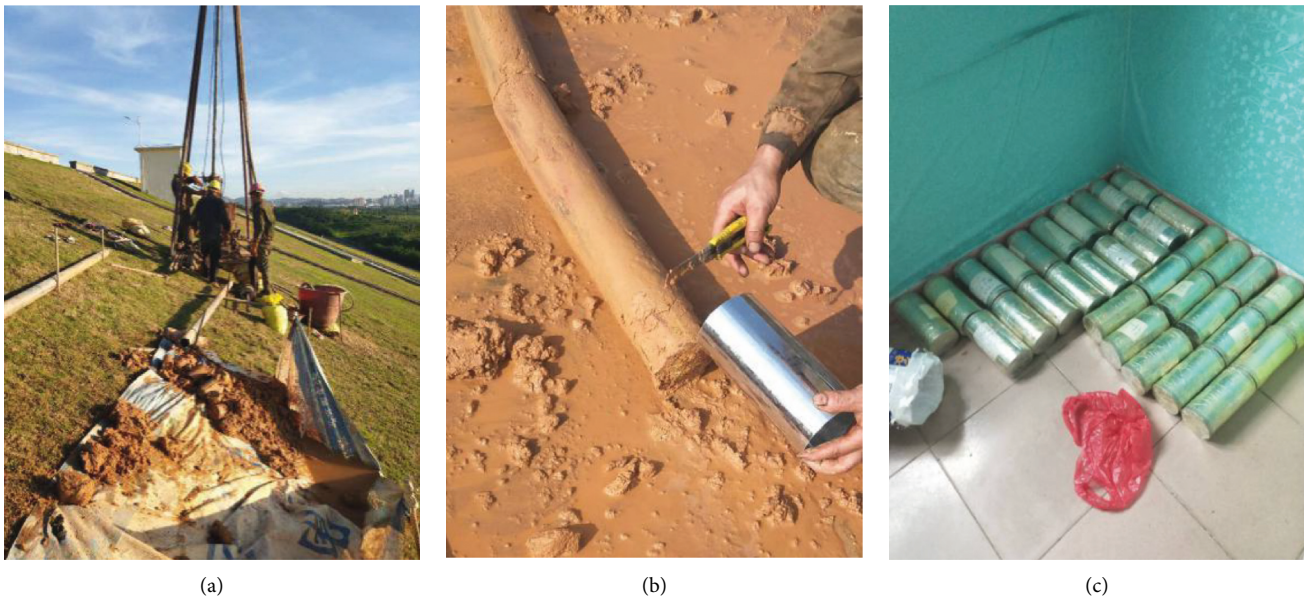
FIGURE 4: Photos of site sampling: (a) well drilling; (b) sampling; (c) specimen.

TABLE 1: Permeability coefficient of different materials of the dam.

Dam materials	Permeability coefficient (cm/s)
Clay core material	1.8×10^{-5}
Shell material	2.1×10^{-5}
Impervious wall material	1.0×10^{-8}
Completely weathering layer material in the base	5.0×10^{-5}
Strongly weathered layer material in the base	1.0×10^{-4}
Weakly weathered layer material in the base	1.0×10^{-5}
Heavy curtain material in the base	1.0×10^{-7}
Inverted layer material	1.0×10^{-3}

establish the element governing equations that satisfy the pore pressure and deformation of the element nodes by the variational method or the weighted residual method; (iv) assemble the element governing equations as a whole in the order of node numbers, and establish an overall finite element equation system with unknown values of pore pressure and deformation of all nodes in the calculation area; (v) obtain the pore pressure value and deformation value of the node by solving the equation system, so as to obtain the pore pressure and deformation distribution of the entire calculation area.

Duncan-Chang model was used to describe the stress-strain relationship of the completely weathered and strongly weathered layer, clay core, and shell materials, while the linear elastic model was used for the weakly weathered layer, heavy curtain, and inverted layer materials. Triaxial tests were carried out on the various materials, and constitutive parameters were obtained, as shown in Table 2. The

TABLE 2: Constitutive parameters of various materials of the dam.

Dam materials	Duncan-Chang model						
	c (kPa)	φ (°)	K	n	R_f	K_b	m
Completely weathering material	47.5	38.3	143.3	0.73	0.745	38.75	0.77
Strongly weathered material	100	38.0	1200	0.28	0.82	1200	0.21
Clay core material	31.0	35.4	152.8	0.73	0.705	41.75	0.73
Shell material	17.3	36.1	123	0.69	0.685	47.8	0.68
Dam materials	Linear elastic model						
	E (GPa)				v		
Impervious wall material	25.5				0.167		
Inverted layer material	20.0				0.2		
Weakly weathered material	18.0				0.2		

permeability coefficients of various materials used in the model are shown in Table 1, where c, φ, K, n, R_f, K_b, and m are parameters in the Duncan-Chang model, and E and v are parameters in the linear elastic model.

5.2. Simulation Model and Boundary Condition. Based on the layout plan of the No. 4 dam cross-section and geological conditions, a three-dimensional finite element analysis model is established for the No. 4 dam, as shown in Figure 5. The model has 15510 divided elements, all of which are 8-node isoparametric elements, and the total number of nodes is 17572. The x-axis direction in Figure 5 is the dam axis direction, the y-axis is the upstream and downstream direction, and the z-axis is the vertical direction. The upstream and downstream range of the model is $-340 \sim 320$ m, and the elevation range is $-130 \sim 63.5$ m. Since the dam crest elevation is 63.5 m, it is reasonable to take the elevation of the top of the model to 63.5 m. The boundary conditions for seepage calculation are taken as follows: the bottom of the dam is regarded as the impervious boundary; the left side is the upstream water head boundary; the right side is the downstream water head boundary. The boundary condition for the stress calculation part is that the bottom of the dam is constrained by the displacement in the x and y directions.

Since the Gongming Reservoir has been in operation for many years, the water level has little changed during the operation, and the dam has basically been in a stable state of consolidation. Therefore, two working conditions of the normal water level and the sharp drop in the storage level (water level suddenly drops from the normal water level to the dead water level) are selected for FEM calculation and analysis.

5.3. Results and Analysis. To verify the rationality of the finite element model and calculation parameters, the phreatic line under the normal storage water level was calculated using the FEM, and the calculated result was compared to the measured value. The measured and calculated phreatic lines of the dam section under the normal water storage condition are shown in Figure 3. The calculated value of the three-dimensional finite element stable seepage is in good agreement with the measured value,
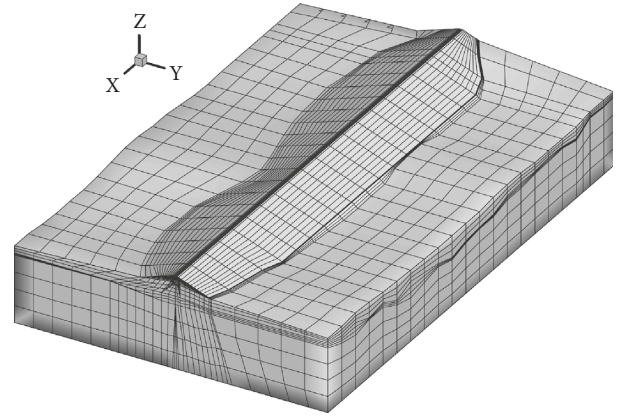
FIGURE 5: Three-dimensional finite element model of the No. 4 dam of Gongming Reservoir.

which proves the rationality of the finite element model and calculation parameters.

Figure 6 shows the cloud map of the major and minor principal stresses and total stress of a certain section of the dam under the normal water storage condition. It can be seen that the major and minor principal stresses of the section are distributed in layers, and they increase with the increase of depth. Since the concrete anti-seepage wall arranged at the dam base cuts off the completely weathered layer of the dam, a large stress is generated in the soil around the anti-seepage wall, as shown in Figure 6(c).

Figure 7 gives the curve of the settlement of the dam crest on the upstream side with time under the condition of the sharp drop in the storage level. When the reservoir water level drops suddenly, the settlement of the dam crest has a gradual increase as a result of the self-weight load of the dam. The process of pore pressure dissipation is almost synchronous with the occurrence of dam crest settlement. When the pore pressure is completely dissipated, the settlement deformation basically stops.

Figures 8–10 present the deformation of the dam at different times under the condition of the sharp drop in the storage level. Due to the water lever dropping from normal storage water level to the dead water lever, the static pore water pressure in the dam above the dead water level is transformed into the excess pore water pressure. With the

(a)

(b)

(c)
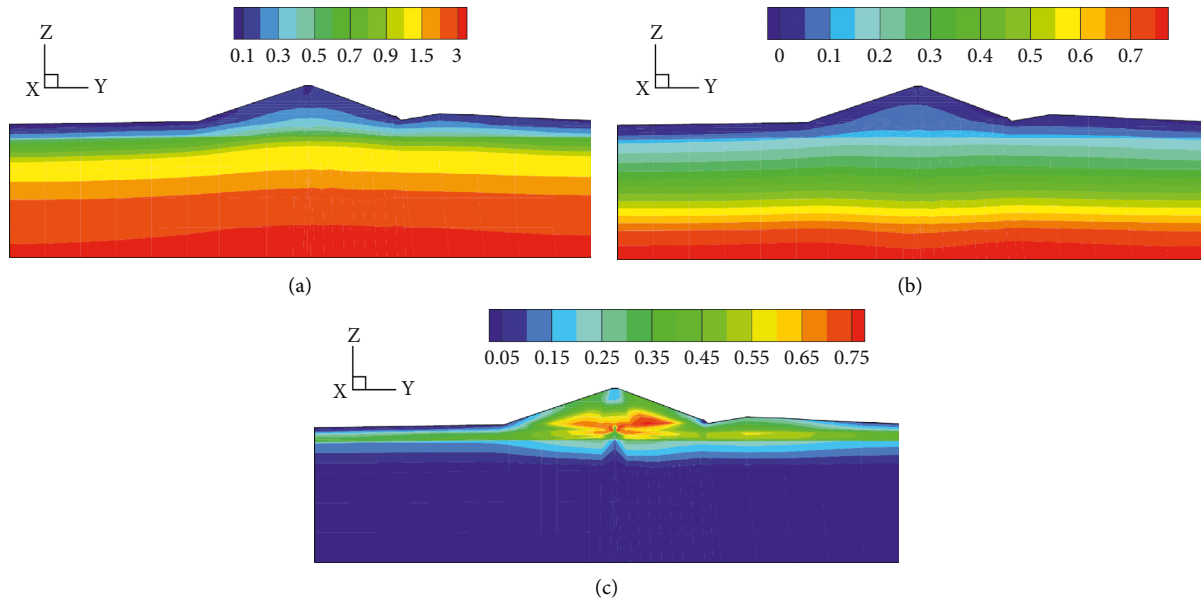
FIGURE 6: Cloud map of stress distribution of dam under the normal storage water level condition (MPa): (a) major principal stress; (b) minor principal stress; (c) total stress.
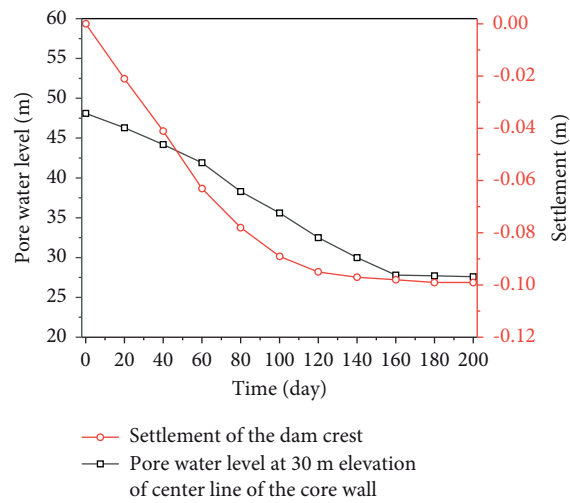
FIGURE 7: Variation curve of dam crest settlement with time after the sharp drop in the storage level.

dissipation of the excess pore water pressure, the effective stress of the dam increases, so only the part of the dam above

(a)

(b)
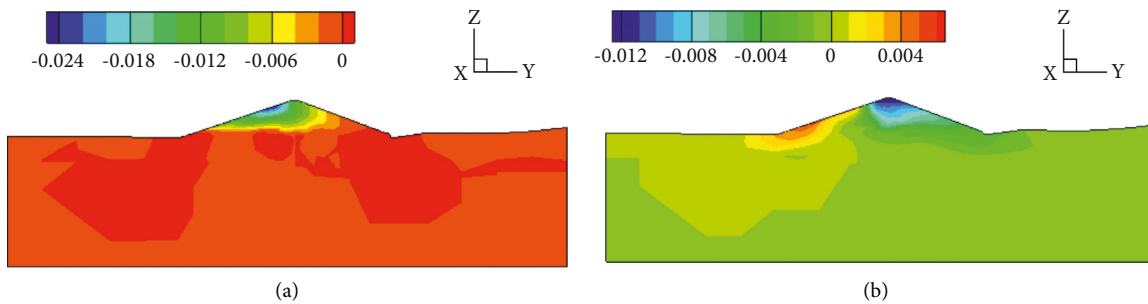
FIGURE 8: Deformation of dam on the 20th day after the sharp drop in the storage level (m): (a) settlement; (b) lateral displacement.

(a)

(b)
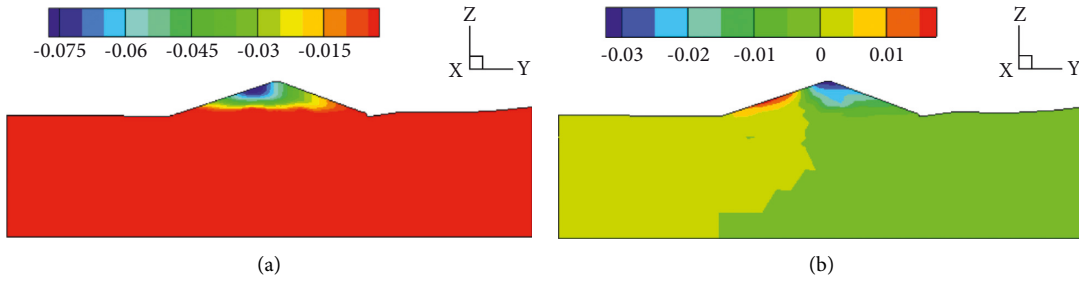
FIGURE 9: Deformation of dam on the 80th day after the sharp drop in the storage level (m): (a) settlement; (b) lateral displacement.

(a)

(b)
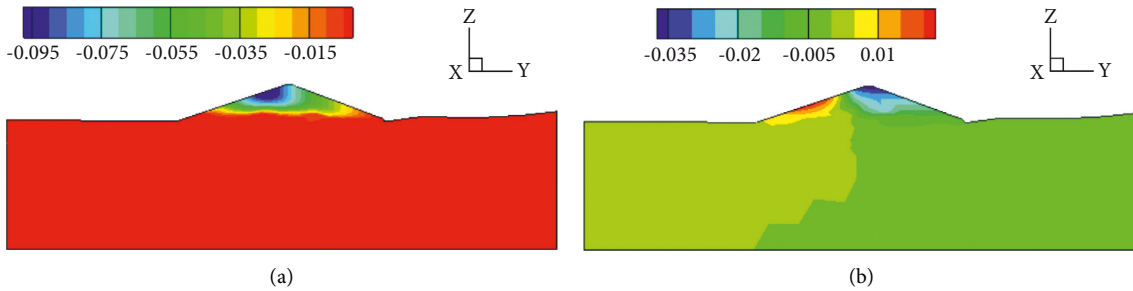
FIGURE 10: Deformation of dam on the 200th day after the sharp drop in the storage level (m): (a) settlement; (b) lateral displacement.

(a)

(b)

(c)
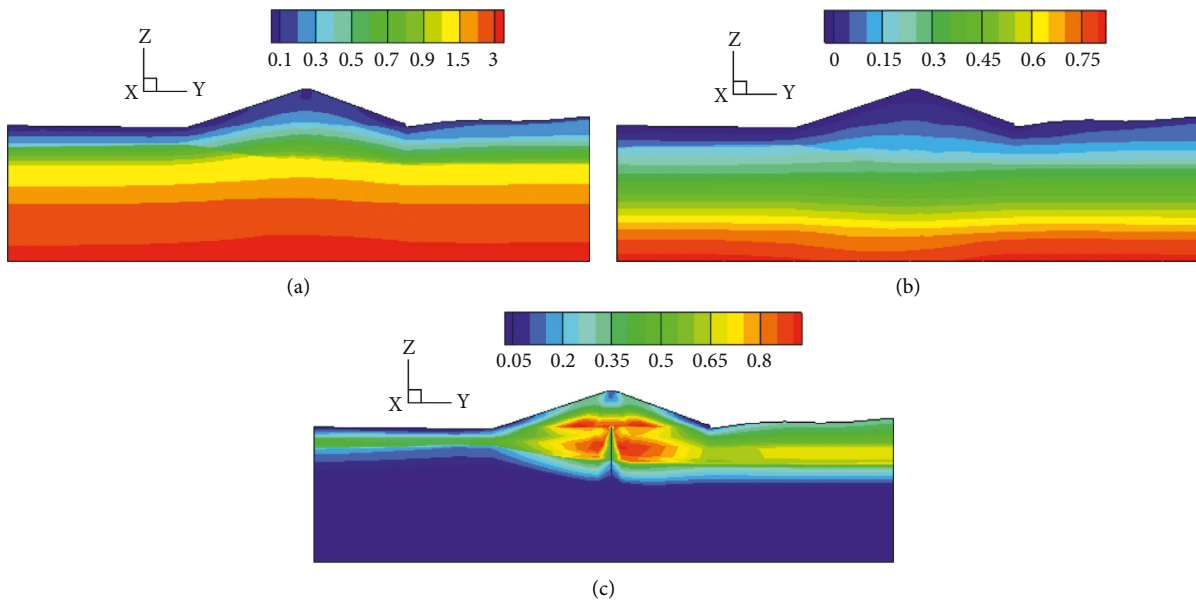
FIGURE 11: Cloud map of stress distribution of dam after the dissipation of the excess pore water pressure (MPa): (a) major principal stress; (b) minor principal stress; (c) total stress.

the dead water level is deformed, which further results in a horizontal displacement upstream of the dam crest and a horizontal displacement downstream of the upstream dam foot. Overall, the deformation of the dam caused by the sharp drop in reservoir water, which is less than 0.1 m, is not large.

Figure 11 shows the cloud map of the major and minor principal stresses and total stress of the dam after the dissipation of the excess pore water pressure. Since the deformation of the dam is small, the effective stress increase caused by the dissipation of pore pressure is not obvious, resulting in that the stress distribution after the dissipation
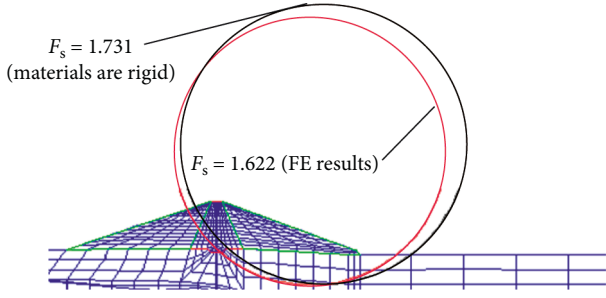
FIGURE 12: The most dangerous sliding surface and safety factor of dam under the normal storage water level.
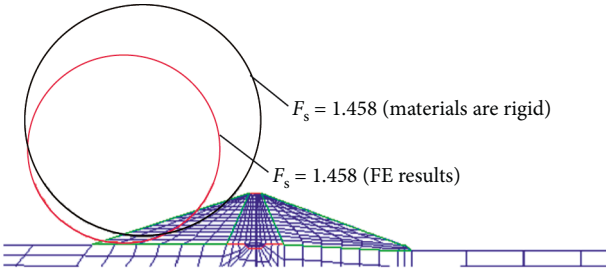
FIGURE 13: The most dangerous sliding surface and safety factor of dam after the dissipation of the excess pore water pressure.

of pore pressure is basically unchanged from that under the normal storage water level.

6. Stability Analysis

At present, the limit equilibrium method is usually used to analyze the stability of the dam analysis, in which the dam material is always assumed to be rigid [17–20]. However, the material is not but has a certain deformation capacity. To evaluate the stability of the dam accurately, the above stresses of the dam under the normal storage water level condition and after the dissipation of the excess pore water pressure calculated by FEM were used to analyze the No. 4 dam stability.

The Bishop method is one of the several methods of slices developed to assess the stability of slopes and derive the associated factor of safety [21–23]. This method combined with the stress calculated by FEM is used to analyze the No. 4 dam stability. The normal stress σ_N and tangential stress τ on the sliding surface can be obtained:

$$\begin{aligned} \sigma_n &= \sigma_y \sin^2 \alpha + \sigma_z \cos^2 \alpha - 2\tau_{yz} \sin \alpha \cos \alpha, \\ \tau &= \tau_{yz}\left(\sin^2 \alpha - \cos^2 \alpha\right) - \left(\sigma_z - \sigma_y\right)\sin \alpha \cos \alpha, \end{aligned} \tag{7}$$

where σ_y, σ_z, and τ_{yz} are the stress components of the simulation result; α is the angle between the sliding surface and the horizontal line. An arc-shaped sliding surface is assumed in the Bishop slice method. The equation calculating the safety factor F_s is expressed as

$$F_s = \frac{\sum(\sigma_{ni} \tan \varphi + c)l_i}{\sum \tau_i l_i}, \tag{8}$$

where l_i is the arc length of the i_{th} soil strip, φ is the friction angle of soil, c is the cohesion of soil, σ_{ni} is the normal stress of the i_{th} soil strip, and τ_i is the shear stress of the i_{th} soil strip.

Figure 12 gives the most dangerous sliding surface and the safety factor of the dam slope under the normal storage water level obtained by using simulation results and by assuming that the dam materials are rigid. Figure 13 gives the most dangerous sliding surface and the safety factor of the dam slope after the dissipation of the excess pore water pressure obtained by using simulation results and by assuming that the dam materials are rigid. It can be seen from Figures 12 and 13 that the position of the sliding surface obtained by the two methods is different, and the safety factor F_s obtained by using simulation results is smaller than that calculated by assuming that the dam materials are rigid. According to the reservoir capacity of Gongming Reservoir and the importance of the water supply object, the project grade is determined as grade II, and the dam grade is determined as grade 2. According to the Chinese standard (SL274-2020), the safety factor under the condition of the sharp drop in the storage level shall not be less than 1.25 for class II dams. The calculated results by two methods ($F_s = 1.327$ and 1.458) meet the requirement, but the safety factor is close to the allowable value.

7. Conclusion

A series of seepage tests were conducted on the dam materials to analyze the leakage causes of the No. 4 clay core rockfill dam, and a three-dimensional finite element stress-seepage coupled calculation model of the dam was established to study the deformation and stresses of the dam under the condition of normal storage water level and the sharp drop in the storage level. Based on the finite element (FE) results, the stability of the dam was analyzed. The conclusions are as follows:

(i) The permeability coefficient of the c clay core material of the No. 4 core rockfill dam in Gongming Reservoir is close to that of the shell material. Therefore, even if the reservoir water level is low, the seepage surface of the dam is still high, resulting in multiple leakages of the dam.

(ii) The deformation of No. 4 core rockfill dam is small under the condition of normal storage water level and the sharp drop in the storage level, and the stress distribution under the condition of the sharp drop in the storage level is basically consistent with that under the condition of normal storage water level.

(iii) The safety factor obtained by using simulation results is smaller than that calculated by assuming that the dam materials are rigid. The calculated results by two methods meet the requirement of the specification, but the safety factor is close to the allowable value.

Data Availability

The data used to support the findings of the study are included in the article.

Conflicts of Interest

The authors declare that they have no conflicts of interest regarding the publication of this paper.

Acknowledgments

References

[1] X. g. Yang and S. C. Chi, "Seismic stability of earth-rock dams using finite element limit analysis," *Soil Dynamics and Earthquake Engineering*, vol. 64, pp. 1–10, 2014.

[2] C. Shen, S. Liu, L. Wang, and Y. Wang, "Micromechanical modeling of particle breakage of granular materials in the framework of thermomechanics," *Acta Geotechnica*, vol. 14, no. 4, pp. 939–954, 2019.

[3] H. Gu, X. Fu, Y. Zhu, Y. Huang, and L. Huang, "Analysis of social and environmental impact of earth-rock dam breaks based on a fuzzy comprehensive evaluation method," *Sustainability*, vol. 12, no. 15, p. 6239, 2020.

[4] S. Chen, Q. Cao, and W. Cao, "Breach mechanism and numerical simulation for seepage failure of earth-rock dams," *Science China Technological Sciences*, vol. 55, no. 6, pp. 1757–1764, 2012.

[5] H. Su, J. Yang, and M. Yang, "Dam seepage monitoring based on distributed optical fiber temperature system," *IEEE Sensors Journal*, vol. 15, no. 1, pp. 9–13, 2015.

[6] Y. Xiang, S. y. Fu, K. Zhu, H. Fang, and Z. Y. Fang, "Seepage safety monitoring model for an earth rock dam under influence of high-impact typhoons based on particle swarm optimization algorithm," *Water Science and Engineering*, vol. 10, no. 1, pp. 70–77, 2017.

[7] Y. Wang, M. Han, B. Wan, and Y. Wan, "Stability evaluation of earth-rock dam reinforcement with new permeable polymer based on reliability method," *Construction and Building Materials*, vol. 320, Article ID 126294, 2022.

[8] R. Flores-Berrones, M. Ramírez-Reynaga, and E. J. Macari, "Internal erosion and rehabilitation of an earth-rock dam," *Journal of Geotechnical and Geoenvironmental Engineering*, vol. 137, no. 2, pp. 150–160, 2011.

[9] X. Fu, C. S. Gu, H. Z. Su, and X. N. Qin, "Risk analysis of earth-rock dam failures based on fuzzy event tree method," *International Journal of Environmental Research and Public Health*, vol. 15, no. 5, p. 886, 2018.

[10] N. A. Alemie, M. D. Wosenie, A. Z. Belew, E. A. Ayele, and W. T. Ayele, "Performance evaluation of asphalt concrete core earth-rock fill dam relative to clay core earth-rock fill dam in the case of Megech Dam, Ethiopia," *Arabian Journal of Geosciences*, vol. 14, no. 24, p. 2712, 2021.

[11] H. Su, J. Ma, R. Wen, and Z. Wen, "Detect and identify earth rock embankment leakage based on UAV visible and infrared images," *Infrared Physics & Technology*, vol. 122, Article ID 104105, 2022.

[12] W. Zhou, J. Hua, X. Chang, and C. Zhou, "Settlement analysis of the Shuibuya concrete-face rockfill dam," *Computers and Geotechnics*, vol. 38, no. 2, pp. 269–280, 2011.

[13] S. h. Liu, Y. Sun, C. M. Shen, and Z. Y. Yin, "Practical nonlinear constitutive model for rockfill materials with application to rockfill dam," *Computers and Geotechnics*, vol. 119, Article ID 103383, 2020.

[14] W. Cen, J. Luo, J. Shamin Rahman, and M. Shamin Rahman, "Slope stability analysis using genetic simulated annealing algorithm in conjunction with finite element method," *KSCE Journal of Civil Engineering*, vol. 24, no. 1, pp. 30–37, 2020.

[15] Q. Hou, H. Li, Y. Hu, S. Qi, and J. Zhou, "Overtopping process and structural safety analyses of the earth-rock fill dam with a concrete core wall by using numerical simulations," *Arabian Journal of Geosciences*, vol. 14, no. 3, pp. 1–12, 2021.

[16] M. A. Biot, "General theory of three-dimensional consolidation," *Journal of Applied Physics*, vol. 12, no. 2, pp. 155–164, 1941.

[17] R. Kalatehjari and N. Ali, "A review of three-dimensional slope stability analyses based on limit equilibrium method," *Electronic Journal of Geotechnical Engineering*, vol. 18, pp. 119–134, 2013.

[18] S. Liu, K. Xu, and S. Xu, "Field study of a retaining wall constructed with clay-filled soilbags," *Geotextiles and Geomembranes*, vol. 47, no. 1, pp. 87–94, 2019.

[19] K. Fan, S. H. Liu, Y. P. Wang, and Y. Wang, "Sliding stability analysis of a retaining wall constructed by soilbags," *Géotechnique Letters*, vol. 9, no. 3, pp. 211–217, 2019.

[20] K. Fan, J. Yan, W. Zou, Z. Lai, and Z. Lai, "Active earth pressure on non-yielding retaining walls with geofoam blocks and granular backfills," *Transportation Geotechnics*, vol. 33, Article ID 100712, 2022.

[21] R. I. Borja, J. A. White, X. Wu, and W. Wu, "Factor of safety in a partially saturated slope inferred from hydro-mechanical continuum modeling," *International Journal for Numerical and Analytical Methods in Geomechanics*, vol. 36, no. 2, pp. 236–248, 2012.

[22] S. H. Jiang, D. Q. Li, Z. J. Cao, C. B. Zhou, and K. K. Phoon, "Efficient system reliability analysis of slope stability in spatially variable soils using Monte Carlo simulation," *Journal of Geotechnical and Geoenvironmental Engineering*, vol. 141, no. 2, Article ID 04014096, 2015.

[23] D. Q. Li, D. Zheng, Z. J. Cao, X. S. Tang, and K. K. Phoon, "Response surface methods for slope reliability analysis: review and comparison," *Engineering Geology*, vol. 203, pp. 3–14, 2016.